



Link between shape dependent lifetimes and thermal escape in quantum dots and rings

H. T. Sullivan and J. H. Cole 

*Chemical and Quantum Physics, and ARC Centre of Excellence in Exciton Science,
School of Science, RMIT University, Melbourne 3000, Australia*

 (Received 24 August 2023; accepted 20 December 2023; published 23 January 2024)

Understanding the optical emission characteristics of semiconductor nanostructures is important when determining their device applicability. Their emission depends on the material and its geometry, but also depends on other processes such as thermal escape from the nanostructure. Although it is widely accepted that scattering involving longitudinal optical phonons is the key process in thermal escape, it remains unclear why some quantum structures thermally emit excitons while others emit uncorrelated electron-hole pairs or single charge carriers. To investigate this phenomenon, we theoretically determine the energy levels and temperature-lifetime relationships of quantum dots and rings. We find that replicating the observed temperature dependence of the exciton lifetime requires both an eigenspectrum and a thermal escape mechanism which are geometry dependent. This suggests that geometry may be a significant factor in determining the dominant thermal escape process in quantum structures.

DOI: [10.1103/PhysRevResearch.6.013086](https://doi.org/10.1103/PhysRevResearch.6.013086)

I. INTRODUCTION

There is a rapidly growing field of technologies that depend on semiconductor nanostructures [1–3]. Quantum dots (QDs) have been central to these technological developments. The applications for QDs range from biological sensing to single photon sources to quantum computation [4–6]. Improvements in fabrication techniques have resulted in the realization of structures that are more complicated than QDs. These include rods, dumbbells, and platelets, to name a few [7–15]. Each quantum structure has its own unique properties and potential device applications.

Of particular interest in the field of semiconductor nanostructures is quantum rings (QRs). While exhibiting a range of novel properties, the most significant quantum mechanical effect studied in QRs is the Aharonov-Bohm (AB) effect [16]. The characteristic AB oscillations have now been realized in a number of QR systems [17–19].

The unique properties that QRs offer make them suitable to a number of applications. For instance, broad-area lasers have been constructed out of stacked layers of QRs [20]. A simple scheme involving the use of electric and magnetic fields has been proposed to trap excitons in QRs [21]. Photonic crystal lattices containing QRs have been demonstrated to act as single photon emitters [22]. QRs have also been of interest to the spintronics community due to their long spin relaxation time [23]. It has been suggested that the additional degrees of freedom in QRs, arising from their geometry, could be utilized for qubit manipulation [24].

An important question pertaining to QRs is explaining their peculiar relationship between temperature and exciton

lifetime. When the temperature is increased above 150 K, excitons in QRs exhibit a sudden increase in lifetime [25,26]. This contrasts with the typically observed behavior of QDs which undergoes a shortening of excitonic lifetime as the temperature is increased [27–30]. This phenomenon has been explained by assuming the many dark states that are energetically close to the bright ground state become thermally populated at higher temperatures. A similar temperature-lifetime relationship has been observed in quantum wells and was similarly attributed to dark states [31].

Alternatively, the temperature-lifetime relationship observed in QRs could be due to the piezoelectric effect [32]. It is argued that the strain in QRs could induce a significant piezoelectric potential which reduces the overlap between the electron and hole wave function. For temperatures above 150 K, these weakly overlapping states may become occupied and, therefore, an increasing lifetime would be observed.

Neither of these explanations take into account thermal escape from the QR and how this would affect its temperature-lifetime relationship. Whether thermal escape is mediated through the ejection of excitons, uncorrelated electron-hole pairs, or as single charge carriers has been shown to have a significant effect on the temperature-lifetime relationship in QDs [33]. While it is not well understood, it is relatively simple to determine which escape mechanism is dominant in any particular system and it has been resolved for a variety of QDs [33–37]. To our knowledge, this property has not been determined for QRs.

In this paper, we employ the finite element method (FEM) to model QDs and QRs that were fabricated by Lin *et al.* [25,26]. The FEM allows for the specific geometry of each structure to be included in our calculations, permitting a meticulous assessment of the influence that the shape of quantum structures has on their energies and wave functions. Performing calculations that are based on the actual geometry of the QRs and not an idealized shape allows us to determine

Published by the American Physical Society under the terms of the Creative Commons Attribution 4.0 International license. Further distribution of this work must maintain attribution to the author(s) and the published article's title, journal citation, and DOI.

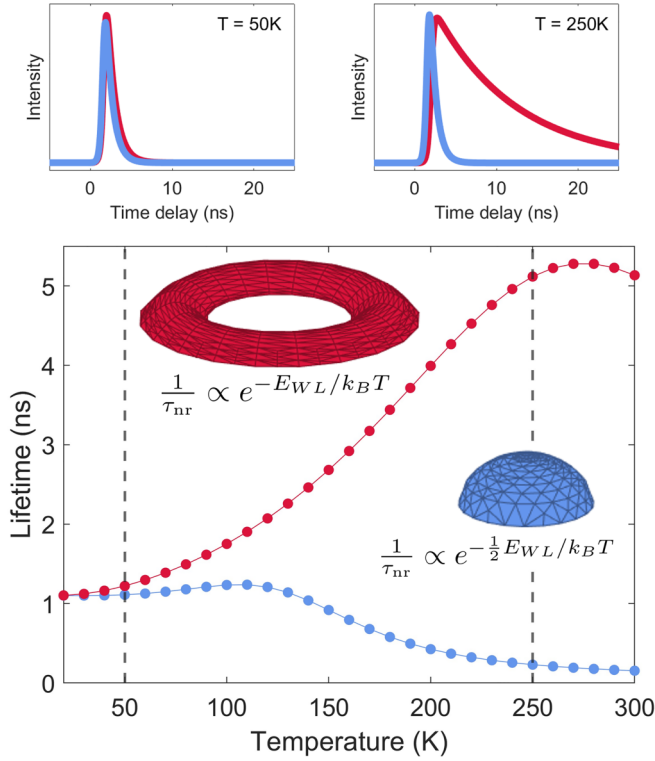


FIG. 1. Conceptual diagram illustrating the temperature dependence of exciton lifetime for quantum dots and quantum rings. The temperature-lifetime relationships of QRs (red) and QDs (blue) are significantly different. The QR undergoes a significant rise in lifetime as temperature is increased, whereas the QD experiences a declining lifetime. Examples of the time-resolved photoluminescence spectroscopy typically seen at 50 K and 250 K are demonstrated above the main figure. This is the measurement that determines the lifetime of the QR and QD. The nonradiative rates ($\frac{1}{\tau_{nr}}$) scale as $\exp(-\nu E_{WL}/k_B T)$, where ν is a parameter that can be determined from the temperature-lifetime relationship. To match published experiments, we find that for QRs $\nu = 1$, which corresponds to exciton emission as the dominant thermal escape mechanism. For the QDs, we find $\nu = 1/2$, which implies thermal emission via uncorrelated electron-hole pairs.

the selection rules of this system and explain the observed photoluminescence (PL) spectra.

The states we calculate are used to determine the temperature-lifetime relationship of the QDs and QRs. We demonstrate that this relationship is highly sensitive to the energy and spacing of the states in each structure and, therefore, is sensitive to the geometry of the system. We also find a shape dependence in the type of thermal emission from each structure. Thus, geometry, through a quantum structure's spectrum of states and thermal emission mechanism, is found to have a significant effect on the lifetime of quantum systems (see Fig. 1).

II. MODELLING QUANTUM DOTS AND QUANTUM RINGS

In this section, we describe how we model QDs and QRs using the FEM. The strength of this technique is that it allows differential equations to be solved across arbitrary geometries.

TABLE I. List of material parameters for the InAs QRs embedded within GaAs which we simulate. The effective mass is in units of the bare electron mass m_0 . The band offsets take into account strain. These values come from Refs. [44,45].

	m_e	m_h	V_e (meV)	V_h (meV)	ϵ_r
InAs	0.023	0.34	0	0	12.37
GaAs	0.067	0.38	513	220	10.86

The flexibility that FEM offers in modeling different shapes has resulted in it being used to investigate a range of quantum structures [38–40].

The set of differential equations we use the FEM to solve are the Schrödinger-Poisson equations. These coupled equations are solved iteratively to account for Coulomb interaction between the electron and hole in excitons. The method involves first solving the Schrödinger equation to determine the wave function of each particle, from which the charge density can be computed. This becomes an input into the Poisson equation which is solved to determine the Coulombic potential that each particle generates. These potentials are then fed back into the Schrödinger equation. The two equations are repeatedly solved until the energies converge,

$$\left(-\frac{\hbar^2}{2m_e}\nabla^2 + V_e(\mathbf{r}) - q|\phi_h|\right)\psi_e(\mathbf{r}) = E_e\psi_e(\mathbf{r}), \quad (1a)$$

$$\left(-\frac{\hbar^2}{2m_h}\nabla^2 + V_h(\mathbf{r}) - q|\phi_e|\right)\psi_h(\mathbf{r}) = E_h\psi_h(\mathbf{r}), \quad (1b)$$

$$\nabla^2\phi_e = -|q|\frac{|\langle\psi_e|\psi_e\rangle|^2}{\epsilon_0\epsilon_r}, \quad (2a)$$

$$\nabla^2\phi_h = -|q|\frac{|\langle\psi_h|\psi_h\rangle|^2}{\epsilon_0\epsilon_r}, \quad (2b)$$

where the effective mass, wave function, energy and Coulomb potential of the electron (hole) is $m_{e(h)}$, $\psi_{e(h)}$, $E_{e(h)}$, and $\phi_{e(h)}$. The potential that the electron (hole) resides in, $V_{e(h)}$, arises from the heterojunction between the quantum structure and the surrounding material. The magnitude of charge of the electron and hole is q . The vacuum and relative permittivity are ϵ_0 and ϵ_r , respectively.

The total energy of an exciton is given by

$$E_{exc} = E_g + E_e + E_h - E_{Coul}, \quad (3)$$

where the band gap is E_g and the energy from the Coulomb interaction is

$$E_{Coul} = -\frac{(E_e^{(0)} - E_e) + (E_h^{(0)} - E_h)}{2}, \quad (4)$$

where $E_{e(h)}^{(0)}$ is the energy of the electron (hole) when initially calculated without the Coulomb interaction. The Schrödinger-Poisson equations double count the Coulomb energy and, hence, the need for this term when computing the total exciton energy.

The material parameters used in our simulations have been recorded in Table I. The effective mass for the hole is taken as the heavy hole mass and we neglect contributions from the light hole. Two band models that exclude the light-hole, like ours, are widely used to model InAs/GaAs nanostructures [1].

Such a model is appropriate for our paper as we primarily aim to explain the temperature-lifetime relationship of QRs. We have found our results are robust to minor shifts in the energies of the electron and hole states, and therefore our conclusions would still hold when a more accurate multiband model is employed [41].

Our simulations were performed using the MATLAB Partial Differential Equation Toolbox with meshes generated in GMSH [42,43]. Each mesh consisted of a nanostructure embedded in a circular prism that extended a minimum 15nm beyond the outside of the QD or QR. The average mesh consisted of approximately 6×10^6 tetrahedral elements.

Employing the FEM requires defining a geometry for each structure. We commence by modeling the QD, as it has a particularly simple structure. The QDs that Lin experiments on are estimated to have an average radius and height of 10 nm and 2 nm, respectively, and they measure the ground state exciton energy to be 1210 meV [26]. We simulate the QD by assuming it is approximately lens shaped with the following height profile: $h(r) = h_0 \cos(\pi r/2R)^{1/2}$ where R is radius of the QD and h_0 is its maximum height. We find that QDs with the same radius as given by Lin but a maximum height $h_0 = 2.35$ nm results in a ground state energy of 1210 meV. The greater height required in our simulations may be attributed to the uncertainty in the QDs dimensions or the extra volume provided by the wetting layer.

Modeling QRs is difficult due to the unevenness in their geometry. This unevenness is largely due to their complicated growth process. QRs are produced by the partial capping of a QD followed by an annealing process that triggers the dot-to-ring transition. This transition has been attributed to the balance of surface free energies on the structure [46,47]. During this transformation, a redistribution of material from the center of the QD outwards generates a ring structure around a crater [48].

It is essential to note that this transition happens anisotropically. QRs often have an elongated radial profile [49,50] or an azimuthally dependent height [40]. While there has been some theoretical work which takes into account the range of asymmetries that can arise in QRs [51], most models employ simple geometries, such as one- or two-dimensional rings [21,52–54], and do not account for deviations away from an idealised geometry.

In this paper, we include various asymmetries that are observed in QRs. However, to provide a foundational understanding of the properties of QRs, we initially model an idealized QR geometry without the added complexity of defects. This simulation takes the dimensions given by Lin *et al.*, that is, an inner radius $R_{in} = 15$ nm and an outer radius $R_{out} = 30$ nm. However, we elect to use a maximum height $h_0 = 2$ nm (instead of the estimated 1nm) to align the ground-state energy with that measured in the PL spectra [25,26]. The radial height profile, between the inner and outer radius, of the QR is given by $h(r) = h_0 \sin(\pi(r - R_{in})/(R_{out} - R_{in}))$. This geometry results in a ground state exciton energy of 1255 meV.

Simulations with this geometry reveal that the electron and hole wave functions are not delocalized across the entire QR, as is typically found in theoretical models of QRs [54–56]. Rather, the electron and the hole are concentrated in one

particular region of the QR. The possibility of the electron and hole localizing in one part of the QR has been previously investigated [53,57]. The mean circumference of the QR is almost an order of magnitude larger than the Bohr radius of InAs (which is 35 m [45]). This inhibits the electron from entirely delocalizing around the QR.

The localization of the electron and hole explain an important feature of the PL spectrum of QRs. That is, the linewidth of the ground state emission is relatively narrow [25,26]. This is not the PL spectrum that is predicted based on simple ring models of QRs. These models produce states that commute with the angular momentum operator and, hence, the wave functions of the electron and hole are separable into vertical, radial, and azimuthal parts of the form $\psi_\ell(r, \theta, z) = R(r)Z(z)e^{i\ell\theta}$, where ℓ corresponds to the angular momentum of the state. These wave functions result in the selection rule $\ell_e + \ell_h = 0$ for radiative recombination between the electron and hole. This implies that many excitons should contribute to the PL spectrum, e.g., $(\psi_e, \psi_h) = (\psi_0, \psi_0), (\psi_1, \psi_{-1}), (\psi_{-1}, \psi_1), (\psi_2, \psi_{-2}),$ etc. As each of these states are typically a few meVs apart, this implies that the PL spectrum should exhibit a very broad peak emerging from the many states near the ground state that can radiatively recombine. As our simulations reveal, QRs do not have states that commute with the angular momentum and, therefore, we expect different selection rules and a different PL spectrum.

We now consider a QR with a defect that enlarges a portion of it. The QRs that Lin fabricates make no mention of elongation or specific azimuthally dependent height function. What is apparent from the atomic force microscopy image is a significant number of imperfections in most of the QRs [25,26]. We systematically explore the effect that different sorts of defects have on the properties of the QRs.

The defects we model involve increasing the height and width of the QR for a portion of the ring. One-half of the QR is extended outwards by following the radius of an ellipse with a maximum distance w beyond the circular radius R_{out} . The expression defining the outer radius for QRs with this sort of defect is

$$R_{out}^{(def)}(\theta) = \begin{cases} \frac{R_{out} + w}{\sqrt{1 + \frac{w^2}{R_{out}^2}(2R_{out} + w)\cos^2(\theta)}}, & \theta \leq \pi \\ R_{out}, & \theta > \pi. \end{cases} \quad (5)$$

The height profile follows the same formula as previously except it is multiplied by an azimuthally dependent factor to account for the unevenness in its height:

$$h^{(def)}(r, \theta) = \begin{cases} h(r)(1 + A \sin^2(\pi\theta/\theta_0)), & \theta \leq \theta_0 \\ h(r), & \theta > \theta_0. \end{cases} \quad (6)$$

With this formulation of the defect, there exists a range of parameters that result in very good agreement with the observed PL spectrum of the QR. For instance, using the parameters $A = 1$, $\theta_0 = \pi$, and $w = 5$ nm results in a ground-state exciton of 1247 meV and a bright exciton at approximately 1293 meV. These two energies closely match the energies of the two bright states found in the PL spectrum. The wave functions of these two excitons are demonstrated in Fig. 2. The geometry of this structure, as well as the QD and idealized QR, are presented in Fig. 3.

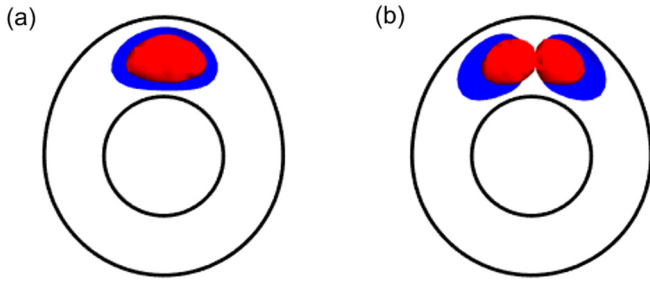


FIG. 2. The electron (blue) and hole (red) wave functions for (a) the ground-state exciton and (b) the first excited state exciton. The two excitons have 1247 meV and 1293 meV, closely matching the experimentally observed bright state energies.

Previous studies have considered geometric anisotropy in QRs in the context of the AB effect [40,58]. This resulted in the ground-state wave function spontaneously localizing in one of the two regions of the QR which was enlarged by the anisotropy. Our idealized model describes the same effect, however, for the sake of simplicity we restrict our study to only one enlarged region. We also computed elongated QRs, and these yielded similar results. In either case, the Coulomb potential deepens the effective potential well in the enlarged region where the electron and hole are localized. This breaks the symmetry of the structure and causes the important low-energy states to reside on that side.

We also used the FEM to calculate the piezoelectric effect. We found that for the dimensions of QRs investigated in this

paper, it had little to no effect. This is consistent with other work that found QRs with large ratios between their outer radius and height would not be significantly influenced by the piezoelectric effect [59].

III. THE TEMPERATURE-LIFETIME MODEL

The relationship between the exciton lifetime of a quantum structure and the temperature depends on its spectrum of states, whether those states are bright or dark and thermal escape mechanisms. Despite this relationship being affected by many parameters and despite there being many different types of QDs, most QDs exhibit approximately the same temperature-lifetime curve [27,30,33,60–62]. At very low temperatures (less than 50 K), it is observed that the lifetime of the system matches the lifetime of the ground-state exciton, typically around 1 ns. This occurs as the system is primarily in the ground state and thermal processes are largely suppressed. Increasing the temperature (typically to around 100 K) results in a slight increase in the lifetime of the QD. This is because the dark states, that are typically tens of meV above the ground state, begin to become occupied and delay radiative recombination. This process is ultimately suppressed at even higher temperatures as thermal escape leading to nonradiative recombination comes to dominate the QD. The increasing contribution from nonradiative recombination is reflected in the reduced PL observed at higher temperatures. Thermal escape reduces the lifetime of the QD until, at approximately room temperature, the lifetime of the QD is effectively unchanged by further increases to temperature.

The relationship for QRs is quite different. At low temperatures, the QR’s lifetime approximately matches the lifetime of the QD. However, from approximately 150 K, instead of the lifetime decreasing there is marked increase in lifetime to about 10.5 ns [25,26].

This phenomenon is attributed to the different spectra of states in QRs and QDs. The QR has many more states close to the ground state which are assumed to be dark states. As the temperature rises, these dark states become thermally populated, thereby increasing the lifetime of the QR. This theory is supported by a two-level rate equation model [25,26].

We construct a more sophisticated model that takes into account the full spectrum of bright and dark excitonic states in each quantum structure. Our model, like other similar models, assumes that the total decay time can be attributed to the radiative and nonradiative lifetimes [61,63,64],

$$\frac{1}{\tau} = \frac{1}{\tau_r} + \frac{1}{\tau_{nr}}, \tag{7}$$

where the radiative and nonradiative lifetimes of the structure are τ_r and τ_{nr} , respectively.

The radiative lifetime of a quantum structure can be calculated by considering the probability each excitonic state is occupied and the probability of that state radiatively recombining. By assuming that the probability of a particular excitonic state being occupied is given by the Boltzmann distribution, the following expression can be given for the

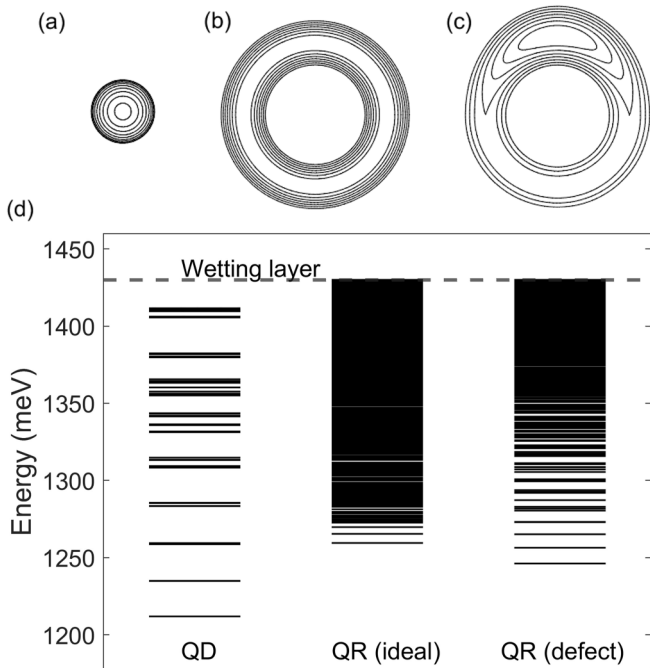


FIG. 3. The geometry of (a) the QD, (b) the idealized QR, and (c) the QR with a defect. The height of each structure is presented as a contour plot where each contour is vertically separated by 0.2 nm. The QR with the defect has the parameters $A = 1$, $\theta_0 = \pi$, and $w = 5$ nm. (d) The energy spectra of each structure where each line represents an excitonic state at a particular energy.

radiative lifetime [61,65,66]:

$$\frac{1}{\tau_r} = \frac{\sum_j^N \Gamma_j e^{-E_j/k_B T}}{Z}, \quad (8)$$

where Γ_j is the radiative recombination rate of the j th excitonic state, Z is the partition function, and N is the number of excitonic states the quantum structure supports.

Our formulation of the radiative lifetime follows the work of Harbord *et al.* [61], however, we extend it by accounting for electron and hole states separately. The probability that an exciton composed of an electron in state i and hole in the state j (which we label as $e_i h_j$) will recombine is given by Fermi's golden rule [1]:

$$\Gamma_{ij} = \frac{2\pi}{\hbar} |\langle i|H|j \rangle|^2. \quad (9)$$

The matrix element for interband transitions in semiconductors is given by the following expression:

$$\langle i|H|j \rangle = p_{cv} \langle i|j \rangle, \quad (10)$$

where p_{cv} is the interband momentum matrix element.

We can relate the radiative rate of the exciton $e_i h_j$ to the radiative rate of the ground-state exciton $e_1 h_1$,

$$\Gamma_{ij} = \Gamma_{11} \frac{|\langle i|j \rangle|^2}{|\langle 1|1 \rangle|^2} = \frac{1}{\tau_0} \frac{|\langle i|j \rangle|^2}{|\langle 1|1 \rangle|^2}, \quad (11)$$

where τ_0 is the lifetime of the ground-state exciton.

We may redefine the radiative lifetime of the system, previously given by Eq. (8), in terms of the electron and hole states,

$$\frac{1}{\tau_r} = \frac{1}{Z_e Z_h \tau_0 |\langle 1|1 \rangle|^2} \sum_i^{N_e} \sum_j^{N_h} |\langle i|j \rangle|^2 e^{-(E_i^{(e)} + E_j^{(h)})/k_B T}, \quad (12)$$

where the partition functions for the electron and hole are defined as

$$Z_e = \sum_i^{N_e} e^{-E_i^{(e)}/k_B T}, \quad (13)$$

$$Z_h = \sum_j^{N_h} e^{-E_j^{(h)}/k_B T}. \quad (14)$$

To simplify the calculation, we set the zero energy for the electron and hole to correspond to the ground state of each charge carrier. In the case where the only bright exciton is the ground-state exciton, the radiative lifetime reduces to a particularly simple expression:

$$\tau_r = Z_e Z_h \tau_0. \quad (15)$$

We calculate the nonradiative lifetime of quantum structures in a similar manner. Our derivation of the nonradiative lifetime follows that of Gurioli *et al.* [63] but we adapt their expression to account for the separate electron and hole states. We assume nonradiative processes predominantly occur when an exciton thermally escapes into the wetting layer. The likelihood that an electron or hole can make this jump depends on the magnitude of the wetting layer energy, E_{WL} . However, it has been demonstrated that the thermal escape rate is modified according to whether it is excitons, uncorrelated electron-hole pairs, or single charge carriers that are emitted [33–37,67,68].

A general escape rate proportional to $\exp(-\nu E_{\text{WL}}/k_B T)$ is typically employed to account for the different escape mechanisms where ν is a fitting factor. By assuming a detailed balance, it has been shown that $\nu = 1$ for exciton emission, $\nu = 1/2$ for uncorrelated pair emission, and $\nu < 1/2$ for single charge carrier emission [33,69]. The importance of including the fitting parameter in our calculations is that it enables us to predict the sort of thermal emission based on which ν value provides the best fit to experimental data.

The total nonradiative rate is determined by the thermal escape rate of each exciton state and the probability of each state being occupied (which we assume is given by the Boltzmann distribution),

$$\begin{aligned} \frac{1}{\tau_{nr}} &= \Gamma_0 \sum_i^{N_e} \sum_j^{N_h} e^{-(\nu E_{\text{WL}}^{(e)} - E_i^{(e)})/k_B T} e^{-(\nu E_{\text{WL}}^{(h)} - E_j^{(h)})/k_B T} \\ &\quad \times \frac{e^{-E_i^{(e)}/k_B T}}{Z_e} \frac{e^{-E_j^{(h)}/k_B T}}{Z_h} \\ &= \frac{\Gamma_0}{Z_e Z_h} \sum_i^{N_e} \sum_j^{N_h} e^{-\nu(E_{\text{WL}}^{(e)} + E_{\text{WL}}^{(h)})/k_B T} \\ &= \frac{\Gamma_0 N_e N_h}{Z_e Z_h} e^{-\nu E_{\text{WL}}/k_B T}, \end{aligned} \quad (16)$$

where the wetting layer energies for the electron and hole are $E_{\text{WL}}^{(e)}$ and $E_{\text{WL}}^{(h)}$, respectively. The total exciton wetting layer energy is $E_{\text{WL}} = E_{\text{WL}}^{(e)} + E_{\text{WL}}^{(h)}$. We assume the wetting layer energy that Lin *et al.* measured in their experiment, $E_{\text{WL}} = 1430 \text{ meV}$. The scattering rate from confined states to the wetting layer is Γ_0 .

Using the formalism presented here and the FEM results of the previous section, we are able to calculate the temperature-lifetime relationship of each structure and its dominant thermal escape mechanism.

IV. THE INTERPLAY OF GEOMETRY AND LIFETIME

The model described in the previous section requires knowledge of the energy levels of the quantum structure being investigated. By combining this model with our FEM results, we are able to determine the temperature-lifetime relationship of each structure. We find that this relationship is sensitive to the geometry. This is because each structure's spectrum depends on its specific shape. The spectra of the QD, idealized QR, and QR with a defect are displayed in Fig. 3.

The temperature-lifetime relationship we calculate for QDs matches the experimentally observed relationship when $\nu = 0.5$. This corresponds to thermal escape primarily by uncorrelated electron-hole pairs, which is consistent with other experiments on QDs [33,35–37]. The relationship for QDs, as well as the idealized QR and the QR with a defect, are presented in Fig. 4.

Our results also demonstrate that the QR with the defect, described in the previous section, has a temperature-lifetime relationship that approximately matches the experimentally observed relationship for the QR [25,26]. This is in stark contrast to the relationship exhibited by the idealized QR which exhibits a significant rise in its lifetime at a

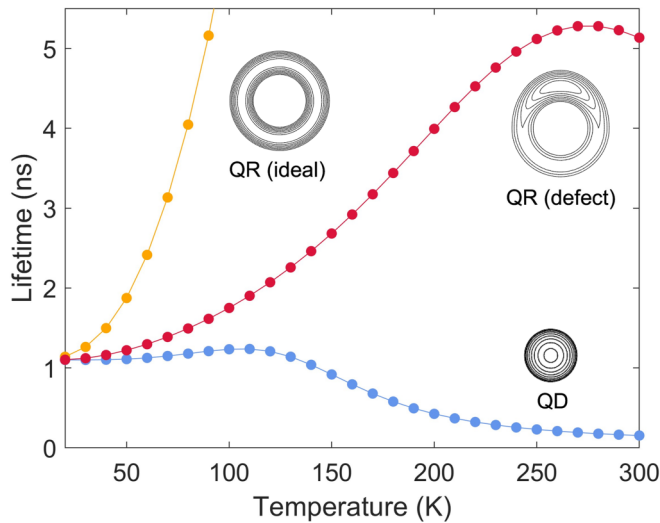


FIG. 4. The lifetimes of the QD, the QR with a defect, and an idealized QR. The emission parameter is $\nu = 0.5$ for the QD and $\nu = 1$ for the QRs. The thermal emission rate is $\Gamma_0 = 10 \text{ ns}^{-1}$ for the QD and $\Gamma_0 = 2 \text{ ns}^{-1}$ for the QRs.

temperature much lower than is experimentally observed. It is worth clarifying why each QR produces a distinct temperature-lifetime relationship.

The marked increase in lifetime at much lower temperatures for the idealized QR can be explained by the proximity of dark states to the ground state, as suggested by Lin *et al.* [25,26]. The spectrum of the idealized QR is illustrated in Fig. 3, revealing the many states close to its ground state. Minimal increases in temperature cause these states to become occupied and, since they are dark states, the occupation of these states increases the lifetime of the system.

The QR with the defect has a significant spacing between its ground state and the next excited state. Its energy spectrum is effectively that of a QD at low energies and that of the idealized QR at higher energies. The consequence of this is that at low temperatures the ground state is primarily occupied, just like in the QD. This results in a large range of temperatures where the QR is most likely in the ground state and, hence, there is only a marginal change to the lifetime in this range. However, once the temperature is reached where the many dark states can be accessed, then there is a sudden increase in lifetime. The defect in the QR provides significant energy spacing around the ground state and the ring geometry provides a close packed set of states at higher energies. Only a spectrum of states with both these features can produce the temperature-lifetime relationship observed for QRs [25,26].

We now consider the type of thermal emission present in QRs. To fit to the experimental results [25,26] requires $\nu = 1$, implying that the thermal emission from QRs involves the ejection of excitons. The temperature-lifetime relationship of QRs with different values of ν is depicted in Fig. 5. The difference in thermal escape mechanisms for QDs and QRs suggests that geometric effects are an important factor in the process. It should be noted that elsewhere it has been calculated that the geometry of QDs significantly effects its capture processes [70,71].

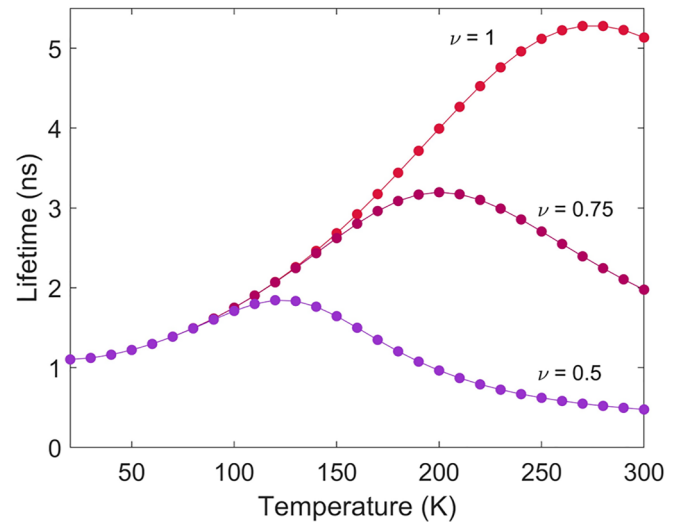


FIG. 5. The lifetimes of the QR with a defect for different ν values. Only when $\nu \approx 1$ does this relationship match what is experimentally observed.

There are some quantitative differences between the temperature-lifetime relationships we calculate and the one measured for QRs. We find that the lifetime of the QR diverges from the lifetime of QD at a lower temperature than is experimentally observed [25,26]. The increased lifetime that we find for the QR arises from the lowest energy dark states being energetically too close to the ground state. However, this sort of spectra did not arise for every defect we investigated. For instance, if we consider a QR with height defect parameters of $A = 1.25$ and $\theta_0 = \pi/2$ but no change to the width ($w = 0$), we find a similar ground-state exciton energy of 1245 meV. Yet this QR has a temperature-lifetime relationship that approximately matches that of the QD up to 150 K, as is experimentally observed for QRs [25,26]. The

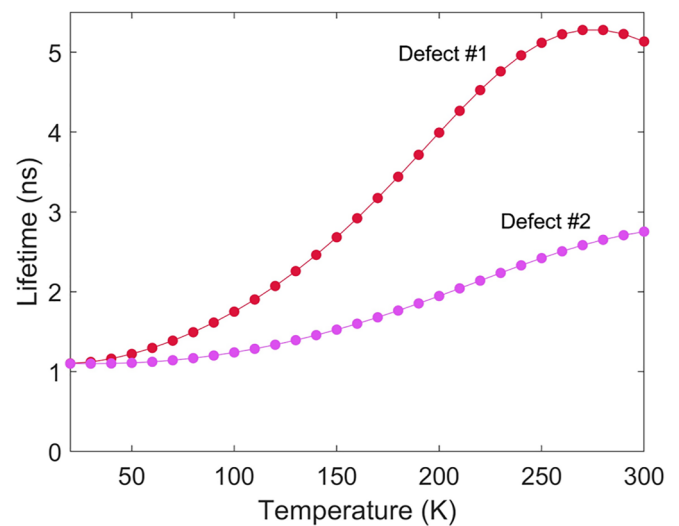


FIG. 6. The lifetime-temperature relationship of two QRs with different defects. The first defect is characterized by $A = 1$, $\theta_0 = \pi$, and $w = 5$; the second defect has the parameters $A = 1.25$, $\theta_0 = \pi/2$, and $w = 0$. We have assumed thermal escape via excitons ($\nu = 1$) for both structures.

maximum lifetime of this QR only reaches 2.75 ns, however, which is well short of the 10.5 ns observed. The temperature-lifetime relationships for these two QRs are demonstrated in Fig. 6.

Nearly every QR with a defect that we modeled, with a ground-state energy that approximately matched the measured PL spectrum, had a temperature-lifetime relationship between the two curves in Fig. 6. To obtain high precision, quantitative agreement would require a detailed model of the materials and any defects, but qualitatively the trends observed are general.

V. CONCLUSION

In this paper, we demonstrate that the distinctive temperature-lifetime relationship observed for QRs is a product of its spectrum of states and its dominant thermal escape mechanism. The spectrum of states required to produce the observed lifetime requires significant energy spacing between states near the ground state but at higher energies' closely packed states. Rotationally symmetric models of QRs

cannot generate this set of states but QRs with defects that enlarge a portion of the ring can.

In matching to the experimentally observed temperature-lifetime relationship, we find that the dominant thermal escape mechanism in QRs involves the ejection of excitons whereas the QDs we investigated thermally emit uncorrelated electron-hole pairs. We therefore suggest that the geometry plays an important role in the thermal escape processes in a quantum structure.

The nature of thermal escape from nanostructures is an ongoing question, but our results suggest the geometric effects are key to understanding this behavior.

ACKNOWLEDGEMENTS

The authors gratefully acknowledge the Australian Research Council (Grant No. CE170100026) and the National Computational Infrastructure (NCI) which is supported by the Australian Government.

-
- [1] P. Harrison and A. Valavanis, *Quantum Wells, Wires and Dots: Theoretical and Computational Physics of Semiconductor Nanostructures* (John Wiley & Sons, New York, 2016).
- [2] A. Orioux, M. A. Versteegh, K. D. Jöns, and S. Ducci, Semiconductor devices for entangled photon pair generation: A review, *Rep. Prog. Phys.* **80**, 076001 (2017).
- [3] P. Michler, *Quantum Dots for Quantum Information Technologies* (Springer, Berlin, 2017), Vol. 237.
- [4] I. L. Medintz, H. T. Uyeda, E. R. Goldman, and H. Mattoussi, Quantum dot bioconjugates for imaging, labelling and sensing, *Nat. Mater.* **4**, 435 (2005).
- [5] P. Senellart, G. Solomon, and A. White, High-performance semiconductor quantum-dot single-photon sources, *Nat. Nanotechnol.* **12**, 1026 (2017).
- [6] D. Loss and D. P. DiVincenzo, Quantum computation with quantum dots, *Phys. Rev. A* **57**, 120 (1998).
- [7] X. Lan, X. Lu, C. Shen, Y. Ke, W. Ni, and Q. Wang, Au nanorod helical superstructures with designed chirality, *J. Am. Chem. Soc.* **137**, 457 (2015).
- [8] F. Pisanello, L. Martiradonna, G. Leménager, P. Spinicelli, A. Fiore, L. Manna, J.-P. Hermier, R. Cingolani, E. Giacobino, M. De Vittorio *et al.*, Room temperature-dipolelike single photon source with a colloidal dot-in-rod, *Appl. Phys. Lett.* **96**, 033101 (2010).
- [9] I. Moreels, G. Rainò, R. Gomes, Z. Hens, T. Stöferle, and R. F. Mahrt, Nearly temperature-independent threshold for amplified spontaneous emission in colloidal CdSe/CdS quantum dot-in-rods, *Adv. Mater.* **24**, OP231 (2012).
- [10] F. Di Stasio, J. Q. Grim, V. Lesnyak, P. Rastogi, L. Manna, I. Moreels, and R. Krahn, Single-mode lasing from colloidal water-soluble CdSe/CdS quantum dot-in-rods, *Small* **11**, 1328 (2015).
- [11] B. Ji, Y. E. Panfil, and U. Banin, Heavy-metal-free fluorescent ZnTe/ZnSe nanodumbbells, *ACS Nano* **11**, 7312 (2017).
- [12] G. Jia, Y. Pang, J. Ning, U. Banin, and B. Ji, Heavy-metal-free colloidal semiconductor nanorods: Recent advances and future perspectives, *Adv. Mater.* **31**, 1900781 (2019).
- [13] S. Ithurria, M. Tessier, B. Mahler, R. P. S. M. Lobo, B. Dubertret, and A. L. Efros, Colloidal nanoplatelets with two-dimensional electronic structure, *Nat. Mater.* **10**, 936 (2011).
- [14] B. Guzelturk, O. Erdem, M. Olutas, Y. Kelestemur, and H. V. Demir, Stacking in colloidal nanoplatelets: Tuning excitonic properties, *ACS Nano* **8**, 12524 (2014).
- [15] B. Guzelturk, Y. Kelestemur, M. Olutas, S. Delikanli, and H. V. Demir, Amplified spontaneous emission and lasing in colloidal nanoplatelets, *ACS Nano* **8**, 6599 (2014).
- [16] Y. Aharonov and D. Bohm, Significance of electromagnetic potentials in the quantum theory, *Phys. Rev.* **115**, 485 (1959).
- [17] A. Lorke, R. J. Luyken, A. O. Govorov, J. P. Kotthaus, J. M. Garcia, and P. M. Petroff, Spectroscopy of nanoscopic semiconductor rings, *Phys. Rev. Lett.* **84**, 2223 (2000).
- [18] M. Bayer, M. Korkusinski, P. Hawrylak, T. Gutbrod, M. Michel, and A. Forchel, Optical detection of the Aharonov-Bohm effect on a charged particle in a nanoscale quantum ring, *Phys. Rev. Lett.* **90**, 186801 (2003).
- [19] U. Keyser, S. Borck, R. Haug, M. Bichler, G. Abstreiter, and W. Wegscheider, Aharonov-Bohm oscillations of a tuneable quantum ring, *Semicond. Sci. Technol.* **17**, L22 (2002).
- [20] F. Suárez, D. Granados, M. L. Dotor, and J. M. García, Laser devices with stacked layers of InGaAs/GaAs quantum rings, *Nanotechnology* **15**, S126 (2004).
- [21] A. M. Fischer, V. L. Campo Jr, M. E. Portnoi, and R. A. Römer, Exciton storage in a nanoscale Aharonov-Bohm ring with electric field tuning, *Phys. Rev. Lett.* **102**, 096405 (2009).
- [22] E. Gallardo, L. Martínez, A. Nowak, D. Sarkar, D. Sanvitto, H. Van der Meulen, J. Calleja, I. Prieto, D. Granados, A. G. Taboada *et al.*, Single-photon emission by semiconductor quantum rings in a photonic crystal, *J. Opt. Soc. Am. B* **27**, A21 (2010).

- [23] E. Zipper, M. Kurpas, J. Sadowski, and M. M. Maška, Spin relaxation in semiconductor quantum rings and dots—a comparative study, *J. Phys.: Condens. Matter* **23**, 115302 (2011).
- [24] E. Zipper, M. Kurpas, M. Szelag, J. Dajka, and M. Szopa, Flux qubit on a mesoscopic nonsuperconducting ring, *Phys. Rev. B* **74**, 125426 (2006).
- [25] C. Lin, H. Lin, C. Huang, S. Su, S.-D. Lin, K.-W. Sun, C. Lee, Y. Liu, M. Yang, and J. Shen, Temperature dependence of time-resolved photoluminescence spectroscopy in InAs/GaAs quantum ring, *Appl. Phys. Lett.* **94**, 183101 (2009).
- [26] C. Lin, H. Ling, S. Su, S.-D. Lin, C. Lee, and K.-W. Sun, Shape dependent carrier dynamics in InAs/GaAs nanostructures, *J. Appl. Phys.* **106**, 113522 (2009).
- [27] R. Heitz, I. Mukhametzhanov, A. Madhukar, A. Hoffmann, and D. Bimberg, Temperature dependent optical properties of self-organized InAs/GaAs quantum dots, *J. Electron. Mater.* **28**, 520 (1999).
- [28] M. De Giorgi, C. Lingk, G. Von Plessen, J. Feldmann, S. De Rinaldis, A. Passaseo, M. De Vittorio, R. Cingolani, and M. Lomascolo, Capture and thermal re-emission of carriers in long-wavelength InGaAs/GaAs quantum dots, *Appl. Phys. Lett.* **79**, 3968 (2001).
- [29] D. Valerini, A. Creti, M. Lomascolo, L. Manna, R. Cingolani, and M. Anni, Temperature dependence of the photoluminescence properties of colloidal CdSe/ZnS core/shell quantum dots embedded in a polystyrene matrix, *Phys. Rev. B* **71**, 235409 (2005).
- [30] C. de Mello Donegá, M. Bode, and A. Meijerink, Size-and temperature-dependence of exciton lifetimes in CdSe quantum dots, *Phys. Rev. B* **74**, 085320 (2006).
- [31] T. J. Badcock, P. Dawson, R. A. Oliver, M. J. Kappers, and C. J. Humphreys, Evidence for dark states in the temperature dependent recombination dynamics of InGaAs/GaAs quantum wells, *Jpn. J. Appl. Phys.* **52**, 08JL12 (2013).
- [32] V. M. Fomin, *Physics of Quantum Rings* (Springer Science & Business Media, Heidelberg, 2013).
- [33] W. Yang, R. R. Lowe-Webb, H. Lee, and P. C. Sercel, Effect of carrier emission and retrapping on luminescence time decays in InAs/GaAs quantum dots, *Phys. Rev. B* **56**, 13314 (1997).
- [34] S. Khatsevich, D. Rich, E.-T. Kim, and A. Madhukar, Cathodoluminescence imaging and spectroscopy of excited states in InAs self-assembled quantum dots, *J. Appl. Phys.* **97**, 123520 (2005).
- [35] W.-M. Schulz, R. Roßbach, M. Reischle, G. J. Beirne, M. Bommer, M. Jetter, and P. Michler, Optical and structural properties of InP quantum dots embedded in $(\text{Al}_x\text{Ga}_{1-x})_{.51}\text{In}_{0.49}\text{P}$, *Phys. Rev. B* **79**, 035329 (2009).
- [36] G. Gélinas, A. Lanacer, R. Leonelli, R. A. Masut, and P. J. Poole, Carrier thermal escape in families of InAs/InP self-assembled quantum dots, *Phys. Rev. B* **81**, 235426 (2010).
- [37] N. A. Jahan, C. Hermannstädter, J.-H. Huh, H. Sasakura, T. J. Rotter, P. Ahirwar, G. Balakrishnan, K. Akahane, M. Sasaki, H. Kumano *et al.*, Temperature dependent carrier dynamics in telecommunication band InAs quantum dots and dashes grown on InP substrates, *J. Appl. Phys.* **113**, 033506 (2013).
- [38] R. Melnik and K. Zotsenko, Finite element analysis of coupled electronic states in quantum dot nanostructures, *Modell. Simul. Mater. Sci. Eng.* **12**, 465 (2004).
- [39] T. Markussen, P. Kristensen, B. Tromborg, T. W. Berg, and J. Mørk, Influence of wetting-layer wave functions on phonon-mediated carrier capture into self-assembled quantum dots, *Phys. Rev. B* **74**, 195342 (2006).
- [40] V. M. Fomin, V. N. Gladilin, S. N. Klimin, J. T. Devreese, N. A. J. M. Kleemans, and P. M. Koenraad, Theory of electron energy spectrum and Aharonov-Bohm effect in self-assembled $\text{In}_x\text{Ga}_{1-x}\text{As}$ quantum rings in GaAs, *Phys. Rev. B* **76**, 235320 (2007).
- [41] T. Chwiej and B. Szafran, Signatures of antibonding hole ground states in exciton spectra of vertically coupled quantum dots in an electric field, *Phys. Rev. B* **81**, 075302 (2010).
- [42] MATLAB and Partial Differential Equation Toolbox 2019b, The MathWorks, Inc., Natick, Massachusetts.
- [43] C. Geuzaine and J. Remacle, Gmsh: A 3-D finite element mesh generator with built-in pre-and post-processing facilities, *Int. J. Numer. Methods Eng.* **79**, 1309 (2009).
- [44] S.-S. Li, J.-B. Xia, Z. L. Yuan, Z. Y. Xu, W. Ge, X. R. Wang, Y. Wang, J. Wang, and L. L. Chang, Effective-mass theory for InAs/GaAs strained coupled quantum dots, *Phys. Rev. B* **54**, 11575 (1996).
- [45] O. Madelung, *Semiconductors: Data Handbook* (Springer Science & Business Media, Heidelberg, 2004).
- [46] R. Blossey and A. Lorke, Wetting droplet instability and quantum ring formation, *Phys. Rev. E* **65**, 021603 (2002).
- [47] S. Kobayashi, C. Jiang, T. Kawazu, and H. Sakaki, Self-assembled growth of GaSb type II quantum ring structures, *Jpn. J. Appl. Phys.* **43**, L662 (2004).
- [48] A. L. J. Luyken, J. M. Garcia, and P. M. Petroff, Growth and electronic properties of self-organized quantum rings, *Jpn. J. Appl. Phys.* **40**, 1857 (2001).
- [49] T. Raz, D. Ritter, and G. Bahir, Formation of InAs self-assembled quantum rings on InP, *Appl. Phys. Lett.* **82**, 1706 (2003).
- [50] T. Kuroda, T. Mano, T. Ochiai, S. Sanguinetti, K. Sakoda, G. Kido, and N. Koguchi, Optical transitions in quantum ring complexes, *Phys. Rev. B* **72**, 205301 (2005).
- [51] J. Vinasco, A. Radu, E. Kasapoglu, R. Restrepo, A. Morales, E. Feddi, M. Mora-Ramos, and C. Duque, Effects of geometry on the electronic properties of semiconductor elliptical quantum rings, *Sci. Rep.* **8**, 13299 (2018).
- [52] A. M. Alexeev and M. E. Portnoi, Electric dipole moment oscillations in Aharonov-Bohm quantum rings, *Phys. Rev. B* **85**, 245419 (2012).
- [53] A. O. Govorov, S. E. Ulloa, K. Karrai, and R. J. Warburton, Polarized excitons in nanorings and the optical Aharonov-Bohm effect, *Phys. Rev. B* **66**, 081309(R) (2002).
- [54] N. F. Hartmann, M. Otten, I. Fedin, D. Talapin, M. Cygorek, P. Hawrylak, M. Korkusinski, S. Gray, A. Hartschuh, and X. Ma, Uniaxial transition dipole moments in semiconductor quantum rings caused by broken rotational symmetry, *Nat. Commun.* **10**, 3253 (2019).
- [55] S. Tomić, A. G. Sunderland, and I. J. Bush, Parallel multi-band k-p code for electronic structure of zinc blend semiconductor quantum dots, *J. Mater. Chem.* **16**, 1963 (2006).
- [56] M. D. Teodoro, V. L. Campo, Jr., V. Lopez-Richard, E. Marega, Jr., G. E. Marques, Y. G. Gobato, F. Iikawa, M. J. S. P. Brasil, Z. Y. AbuWaar, V. G. Dorogan, Y. I. Mazur, M. Benamara, and

- G. J. Salamo, Aharonov-Bohm interference in neutral excitons: Effects of built-in electric fields, *Phys. Rev. Lett.* **104**, 086401 (2010).
- [57] H. Kim, W. Lee, S. Park, K. Kyhm, K. Je, R. A. Taylor, G. Nogues, L. S. Dang, and J. D. Song, Quasi-one-dimensional density of states in a single quantum ring, *Sci. Rep.* **7**, 1 (2017).
- [58] V. Fomin, V. Gladilin, J. Devreese, N. Kleemans, M. Bozkurt, and P. Koenraad, Electron and exciton energy spectra in self-assembled InGaAs/GaAs ring-like nanostructures, *Phys. Status Solidi B* **245**, 2657 (2008).
- [59] J. A. Barker, R. J. Warburton, and E. P. O'Reilly, Electron and hole wave functions in self-assembled quantum rings, *Phys. Rev. B* **69**, 035327 (2004).
- [60] S. Sauvage, P. Boucaud, R. P. S. M. Lobo, F. Bras, G. Fishman, R. Prazeres, F. Glotin, J. M. Ortega, and J.-M. Gérard, Long polaron lifetime in InAs/GaAs self-assembled quantum dots, *Phys. Rev. Lett.* **88**, 177402 (2002).
- [61] E. Harbord, P. Spencer, E. Clarke, and R. Murray, Radiative lifetimes in undoped and p-doped InAs/GaAs quantum dots, *Phys. Rev. B* **80**, 195312 (2009).
- [62] D. Oron, A. Aharoni, C. de Mello Donega, J. van Rijssel, A. Meijerink, and U. Banin, Universal role of discrete acoustic phonons in the low-temperature optical emission of colloidal quantum dots, *Phys. Rev. Lett.* **102**, 177402 (2009).
- [63] M. Gurioli, J. Martinez-Pastor, M. Colocci, C. Deparis, B. Chastaing, and J. Massies, Thermal escape of carriers out of GaAs/Al_xGa_{1-x} As quantum-well structures, *Phys. Rev. B* **46**, 6922 (1992).
- [64] M. T. Man and H. S. Lee, Discrete states and carrier-phonon scattering in quantum dot population dynamics, *Sci. Rep.* **5**, 8267 (2015).
- [65] T. Takagahara, Nonlocal theory of the size and temperature dependence of the radiative decay rate of excitons in semiconductor quantum dots, *Phys. Rev. B* **47**, 16639 (1993).
- [66] H. Gotoh, H. Ando, and T. Takagahara, Radiative recombination lifetime of excitons in thin quantum boxes, *J. Appl. Phys.* **81**, 1785 (1997).
- [67] G. Bacher, H. Schweizer, J. Kovac, A. Forchel, H. Nickel, W. Schlapp, and R. Lösch, Influence of barrier height on carrier dynamics in strained In_xGa_{1-x}As/GaAs quantum wells, *Phys. Rev. B* **43**, 9312 (1991).
- [68] G. Muñoz-Matutano, I. Suárez, J. Canet-Ferrer, B. Alén, D. Rivas, L. Seravalli, G. Trevisi, P. Frigeri, and J. Martínez-Pastor, Size dependent carrier thermal escape and transfer in bimodally distributed self assembled InAs/GaAs quantum dots, *J. Appl. Phys.* **111**, 123522 (2012).
- [69] P. Michler, A. Hangleiter, M. Moser, M. Geiger, and F. Scholz, Influence of barrier height on carrier lifetime in Ga_{1-y}In_yP/(Al_xGa_{1-x})_{1-y}In_yP single quantum wells, *Phys. Rev. B* **46**, 7280 (1992).
- [70] I. Magnúsdóttir, A. V. Uskov, S. Bischoff, B. Tromborg, and J. Mørk, One- and two-phonon capture processes in quantum dots, *J. Appl. Phys.* **92**, 5982 (2002).
- [71] I. Magnúsdóttir, S. Bischoff, A. V. Uskov, and J. Mørk, Geometry dependence of auger carrier capture rates into cone-shaped self-assembled quantum dots, *Phys. Rev. B* **67**, 205326 (2003).